

Freestanding Aligned Multi-walled Carbon Nanotubes for Supercapacitor Devices

JOÃO VITOR SILVA MOREIRA,¹ EVALDO JOSÉ CORAT,²
PAUL WILLIAM MAY,³ LAYS DIAS RIBEIRO CARDOSO,²
PEDRO ALMEIDA LELIS,¹ and HUDSON ZANIN^{1,4,5}

1.—Laboratory of Energy Storage and Supply, Universidade do Vale do Paraíba, Av. Shishima Hifumi 2911, Sao Jose dos Campos, SP CEP 12244-000, Brazil. 2.—National Institute for Space Research, Av. dos Astronautas 1758, Sao Jose dos Campos, SP CEP 12227-010, Brazil. 3.—School of Chemistry, University of Bristol, Bristol BS8 1TS, UK. 4.—Carbon Sci-Tech Labs, Universidade Estadual de Campinas, Av. Albert Einstein, 400, Campinas, SP CEP 13083-852, Brazil. 5.—e-mail: hudsonzanin@gmail.com

We report on the synthesis and electrochemical properties of multi-walled carbon nanotubes (MWCNTs) for supercapacitor devices. Freestanding vertically-aligned MWCNTs and MWCNT powder were grown concomitantly in a one-step chemical vapour deposition process. Samples were characterized by scanning and transmission electron microscopies and Fourier transform infrared and Raman spectroscopies. At similar film thicknesses and surface areas, the freestanding MWCNT electrodes showed higher electrochemical capacitance and gravimetric specific energy and power than the randomly-packed nanoparticle-based electrodes. This suggests that more ordered electrode film architectures facilitate faster electron and ion transport during the charge–discharge processes. Energy storage and supply or supercapacitor devices made from these materials could bridge the gap between rechargeable batteries and conventional high-power electrostatic capacitors.

Key words: Carbon, supercapacitor, aligned, transport, electrochemical cell, nanotube

INTRODUCTION

Electrochemical capacitors (also called supercapacitors or ultracapacitors) are an emerging energy-storage technology that offers high power, short charging time, high safety, and long cycle life, as well as being environmental friendly.¹ Supercapacitors can be used either alone as a primary power source or as an auxiliary power source with rechargeable batteries for high power applications, such as hybrid/electric vehicles.² Carbon supercapacitors are energy-storage devices that use ion adsorption on the surface of highly porous materials to store charge.³ These devices exploit the electrostatic separation between electrolyte ions and high-

surface-area electrodes, and are often fabricated from microstructured carbon-based materials.³

Electrodes constructed from carbon-based materials have the advantages of fairly low charge transfer impedance and high chemical stability in strongly acidic or alkaline solutions, together with good performance over a wide range of temperatures.^{4–6} Carbon materials can be prepared in various microtextures from powders to freestanding fibres, foams, amorphous, crystals and composites.^{7,8} Carbon nanotubes (CNTs),^{9,10} carbon nanofibres,^{11,12} carbon trees,¹³ fullerenes,¹⁴ the C_n family,¹⁵ carbon onions^{16,17} and carbon spheres¹⁸ have all been investigated as electrodes. Electrodes fabricated from oriented arrays of CNTs, aligned perpendicular to the current collectors, can readily be prepared with large surface areas, high packing densities, and ordered pore networks. These morphological properties are expected to facilitate rapid

charge/discharge kinetics and thereby give high power.¹

Cyclic voltammetry (CV) and chronopotentiometry are complementary tools for supercapacitor device investigation. In CV the cell potential is increased at a certain ramp-rate while the resulting current from faradaic processes is monitored as a function of time. In chronopotentiometry, the current is fixed and we measure the transient of potential. The total charge accumulated at the electrode surface can be found by integrating the electric current with respect to time, while the capacitance can be estimated as the total charge divided by the "potential window".¹⁹ Capacitance is typically measured at different scan rates to characterize the performance of energy storage devices. The capacitance measured at low scan rates is maximum and close to the capacitance under equilibrium conditions.¹⁹

Stoller and Ruoff²⁰ presented a critical review of best-practice test methods that accurately predict a material's performance for a wide range of material sample types and quantities. From that work there are few points we want to highlight: (1) cell capacitance, C , is best determined from galvanostatic or constant current (CC) discharge curves using the measured value for the discharge current, I , and $C = I/(dV/dt)$, where dV/dt is determined from the slope of the CC discharge curve; (2) very low rates of discharge also lead to order-of-magnitude errors, especially when coupled with small electrode masses (at least 10 or more mg); (3) a three-electrode cell is valuable for determining electrochemical-specific material characteristics, whereas a two-electrode test cell is preferred to mimic the physical configuration, internal voltages and charge transfer that occur in a packaged supercapacitor and thus provides the best indication of an electrode material's performance.

Wang et al.²¹ reported on porous graphitic material for high-rate electrochemical capacitive energy storage. The electrodes were a three-dimensional (3D) architecture composed of self-supported macroporous cores and mesoporous walls that could reduce nanoparticle aggregation. The authors claim the physicochemical properties of the electrolyte inside the macropores are similar to those of the bulk electrolyte with the lowest resistance. Ion-buffering reservoirs may be formed in the macropores to minimize the diffusion distances to the interior surfaces. Furthermore, the mesoporous walls provide low-resistance pathways for the ions, while the micropores strengthen the electric-double-layer capacitance. They obtained gravimetric specific energy about few Wh kg^{-1} , depending on the current densities used.

Demarconnay et al.²² reported that a symmetric active-carbon supercapacitor in Na_2SO_4 aqueous solution could operate up to a potential of 1.6 V with a good charge/discharge cyclability. This result is important because the gravimetric specific energy

(E) depends on the operating potential, V , as $E = \frac{1}{2}CV^2$. Cells with aqueous electrolytes are usually cheaper, environment friendly and easy to construct; however, the maximum voltage V in most two-electrode set-ups is normally <1 V due to water splitting, while it reaches 2.7 V in some organic media.

Biswas and Drzal²³ reported an approach to prepare low impedance graphene electrodes which exhibited high ionic and electronic transport due to the combined presence of the fibrous network of polypyrrole and electrically conductive graphene nanosheets. Impedance analysis showed there was a low equivalent series resistance obtained from the interlayer charge transport between the large graphene basal plane and the π conjugated polymer chain. This transport improvement resulted in a high specific capacitance and high gravimetric specific energy storage.

Ge et al.²⁴ reported on triple networks of macroporous electrodes combining single-walled carbon nanotubes (SWCNTs) wrapped around cellulose fibres as the conductive skin, all covered by polyaniline (PANI). The electrodes were highly capacitive, which could be attributed to the synergistic effect between electron transport within the SWCNT network and fast charge transfer in the PANI nanoribbons. A H_3PO_4 /polyvinyl alcohol (PVA) gel was used as the electrolyte and pristine cellulose paper was used as the separator between two electrodes.

In this work we extend these ideas, and use a two-electrode setup with high-mass, randomly packed and oriented multi-walled carbon nanotube (MWCNT) nanoparticle-based electrodes in a PVA gel solution to improve charge transport and consequently increase capacitance and energy storage.

EXPERIMENTAL

Chemicals and Solutions

Polyvinyl alcohol (PVA), phosphoric acid (H_3PO_4), camphor ($\text{C}_{10}\text{H}_{16}\text{O}$), ferrocene ($\text{C}_{10}\text{H}_{10}\text{Fe}$), hydrochloric acid (HCl) and sulfuric acid (H_2SO_4) were used. The electrolyte was prepared with PVA 10% in deionized water at 90°C, and 8% of the solution volume was diluted in concentrated phosphoric acid (H_3PO_4 /PVA/ H_2O) in a beaker, resulting in a gel-like appearance. This type of electrolyte is easier to handle, avoiding leaking and cell malfunction.

Materials Preparation

The MWCNTs were prepared using a mixture of camphor (85 wt.%) and ferrocene in a modified thermal chemical vapour deposition (CVD) furnace. The mixture was vaporized at 220°C in an antechamber, and then the vapor was carried by a nitrogen gas flow to the chamber of the CVD furnace set at 850°C and atmospheric pressure.²⁵ The

vapours quickly flowed into the chamber, which had a flattened region to confine them in the reactive volume. The conditions chosen were optimised to convert these organic vapours into MWCNT powders and flakes. The macroscopic flakes were composed of freestanding aligned MWCNTs and were grown onto the walls of the chamber. By gravitational force, these MWCNTs were stripped off the walls of the furnace during the growth process, and fell to the bottom of the reactor, where they could be collected after the growth run. The time elapsed during the process used to produce the MWCNT was only a few minutes. After preparation, the samples were subject to sonication for 5 h in 10 M of HCl at 150°C, and then they were washed extensively in water and dried.²⁶ Acid etching performed the removal of the iron-based (from ferrocene) catalytic particles from the MWCNT powder and freestanding material. We previously reported that, based upon XPS analysis, this process succeeded in almost complete removal of external iron content.²⁷

The deliberate incorporation of oxygen-containing groups onto the MWCNT surfaces was carried out in a pulsed direct-current plasma reactor with an oxygen flow rate of 1 sccm, at a pressure of 300 mTorr, -700 V and with pulse frequency of 20 kHz for 30 min.²⁸ The MWCNT powders were oxidized using an in situ stirring system, allowing the oxygen plasma three-dimensional access to the samples. The MWCNT powder deagglomerated during this process. This stirring system worked as a hollow cathode, forming a dense oxygen plasma throughout the entire internal volume. The final freestanding material has its surfaces functionalized by oxygen.

Materials Characterization

The samples were characterized by a variety of methods. Brunauer–Emmett–Teller (BET) surface area measurements were carried out using Quantachrome NovaWin model 1000 for multi-point BET using the classical helium-void volume method. A Krüss Easy Drop system utilizing the sessile drop method measured the contact angle (CA) using high purity deionized water to evaluate the wettability of samples. All measurements were performed at room temperature with as-grown and oxygen functionalized samples. The samples were characterized by transmission electron microscopy (TEM) using a JEOL 3010 microscope adjusted to 300 kV and 120 μ A, using a LaB₆ filament. For TEM images, the samples were pulverized, dispersed in ethanol, and then drop-cast onto a copper mesh coated with carbon film. Images were taken using a JEOL6330F field emission scanning electron microscope (SEM) to evaluate structural arrangements and to monitor details of the surface morphology. We used energy dispersive x-ray spectrometry (EDS) for chemical analysis, operating with a Si(Li) detector with an energy resolution of 126 eV coupled with the SEM.

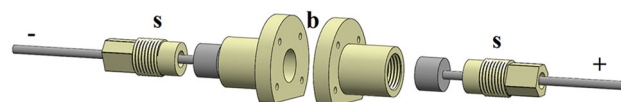


Fig. 1. The electrochemical supercapacitor cell. Letters stand for seals (s), main body of cell (b) and symbols ($-$ or $+$) for electrical contacts.

X-ray photoelectron spectra (XPS) were obtained from powdered samples pressed into a thin film pellet and fixed on a stainless steel holder with conducting double-sided adhesive tape. Raman scattering spectroscopy (Renishaw *invia*) with excitation by Ar⁺-ion laser ($\lambda = 514.5$ nm) in backscattering geometry was used to analyse the structure and changes in the samples. The curve fitting and data analysis software *Fityk* was used to assign the peak locations and fit all spectra.

Electrochemical Set-Up

Electrochemical Cell

The electrochemical supercapacitor cell used in this work was composed the main body and two seals, all made of polyacrylate, which is a hard and low-cost polymer (shown in yellow in Fig. 1). The main body is in two halves which could be bolted together to form a leak-proof cavity containing the collectors. Stainless steel (shown in grey in Fig. 1) was used for the collectors, which were attached to metal rods which passed through the seals and connected externally to the electrical contacts. The cell was employed for the encapsulation of the carbon electrode samples and device consolidation. The design of this cell makes it particularly easy to handle due to the ease with which the samples, the electrolyte and the separators can be replaced or altered.

Electrochemical Assays

Two identical electrodes of 25 mg were coated with the thin solid electrolyte and connected to each other in parallel.²⁹ The working electrode and counter electrode were separated by mesoporous paper inside the electrochemical supercapacitor cell, creating an overall device controlled by an Autolab PGSTAT302N.

The devices were characterized by CV and galvanostatic charge–discharge (g-C/D) in a two-electrode cell set-up. The CV measurements were carried out from 1 mV s⁻¹ to 1000 mV s⁻¹ and between 0 V and 1.0 V. The g-C/D measurements were performed between 0 V and 1.0 V using different electric current values.

RESULTS AND DISCUSSION

Material Characterization

MWCNT powder and freestanding flakes were grown in the same process simultaneously. After

that they were cleaned to remove both external iron oxides and amorphous carbon, and functionalized to incorporate oxygen surface functional groups, all requirements for increasing the capacitance of the bulk material in supercapacitor devices. Most material characterization showed the same results for the powder and the freestanding materials, and in these cases the data are presented only once.

Raman spectra of the powder and freestanding materials (Fig. 2) are very similar, as expected for (a) as-grown and (b) functionalized samples. The Raman spectra were deconvoluted using peaks centred at $\sim 1250\text{ cm}^{-1}$, D ($\sim 1350\text{ cm}^{-1}$), $\sim 1480\text{ cm}^{-1}$, G ($\sim 1580\text{ cm}^{-1}$), D' ($\sim 1611\text{ cm}^{-1}$) and G' ($\sim 2700\text{ cm}^{-1}$, also known as 2D) bands. The D -band is associated with a double-resonance process involving a phonon and a defect, commonly observed in disordered nanoscale carbon phases.³⁰ This observation is consistent with the SEM images (Fig. 3) showing large numbers of edges and boundaries present in the film. The G -band stems from in-plane vibrations and has E_{2g} symmetry corresponding to stretching vibrations in the basal plane (sp^2 domains) of graphene or nanocrystalline graphite.³¹ Generally, the intensity ratio of D and G bands (I_D/I_G) is used to evaluate the degree of disorder of graphitic materials.³² The I_D/I_G ratio of as-grown MWCNT is 0.65 and that of functionalized MWCNT samples is 0.51, which means the treatment was effective in removing amorphous carbon from CNT surfaces.

A high intensity G' band is indicative of highly ordered nanographite.³⁰ The $I_{G'}/I_G$ for as-grown and functionalized samples increased from 0.78 to 1.03, indicating efficient carbon oxidation. Additionally, the feature at $1220\text{--}1280\text{ cm}^{-1}$ has its origin in a double-resonance process on graphene-phonon dispersion curves,³⁰ and this feature increased with functionalization. The band centred at around 1480 cm^{-1} also increased, which is evidence of oxygen functional group attachment to carbon. Indeed, the combination of plasma treatment and

non-oxidative acid treatment damages the CNT wall surfaces, creating reactive dangling bonds allowing incorporation of oxygen functional groups.^{30,33} Although functionalization creates some damaged areas on the CNT sidewalls (Fig. 3a and b), the Raman spectra indicate that oxidation dominates. Results are very similar for the powder and freestanding samples. In summary, Raman analyses indicate mainly the presence of highly crystalline carbon, such as graphene/CNT, together with oxygen groups attached to the surface.

Figure 3a shows TEM micrographs of as-grown MWCNTs exhibiting a crystalline bamboo-like structure with diameters ranging from 20 nm to 40 nm. The nanotubes have an interplanar spacing of $\sim 0.33\text{ nm} \pm 0.02\text{ nm}$ and encapsulate the catalytic iron precursor particles. Figure 3b shows that the functionalised MWCNTs have defective walls and pits caused by the acid treatment and oxidation. The geometric surface areas were measured by BET and helium pycnometry to be $\sim 40.8\text{ m}^2\text{ g}^{-1}$ for freestanding samples and $\sim 38\text{ m}^2\text{ g}^{-1}$ for MWCNT powder.

Figure 4 and Table I present EDS data of as-grown and functionalized MWCNTs. Results are very similar for the powder and freestanding samples, and are discussed below emphasizing the

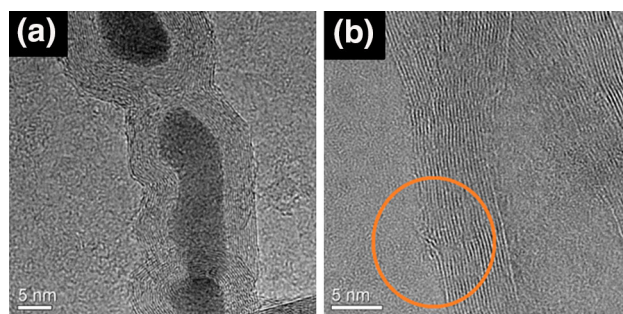


Fig. 3. TEM images of (a) as grown and (b) functionalized MWCNT samples.

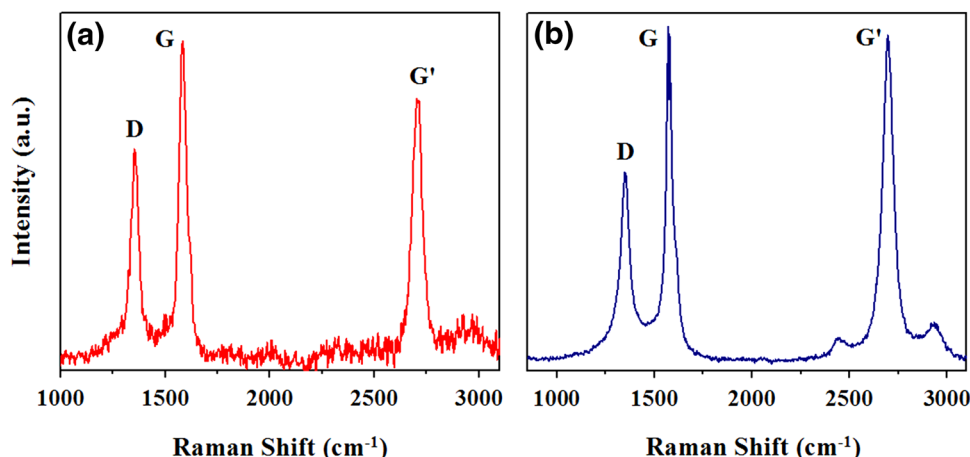


Fig. 2. Raman spectra using 514 nm laser excitation from (a) as-grown and (b) functionalized MWCNT electrodes.

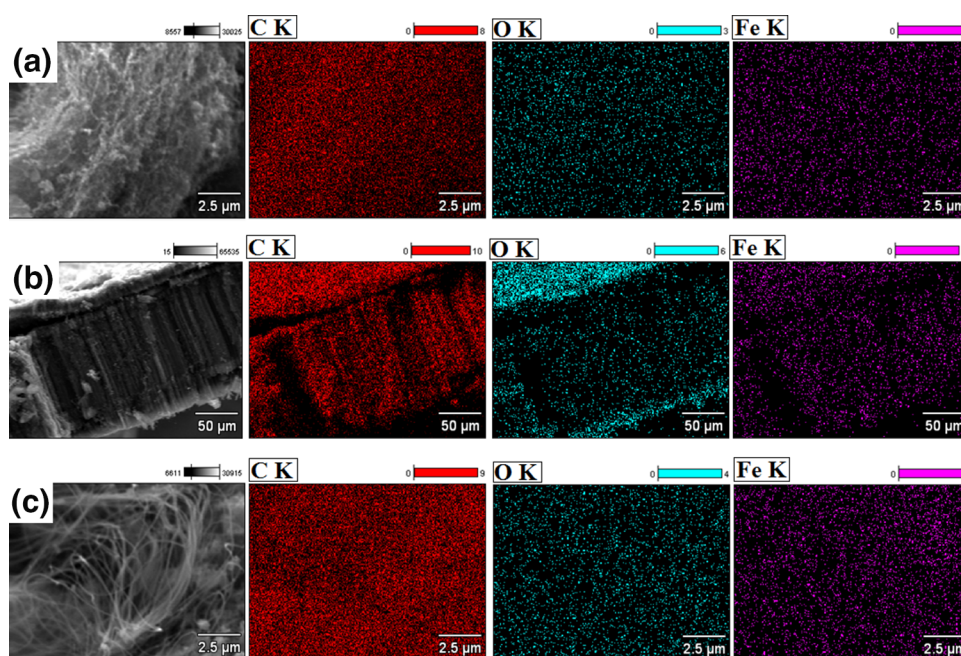


Fig. 4. EDS mapping of the surface of MWCNT (a) before and (b and c) after functionalization. The first column shows the TEM image, with columns 2–4 showing the element maps for C, O and Fe, respectively.

Table I. EDS K-series data from as-grown and functionalized multi-walled carbon nanotubes (MWCNT)

Element	Atomic number	at. %	Uncertainty (1σ) at. %
As-grown MWCNT			
C	6	88.97	10.97
O	8	1.29	0.70
N	7	1.6	1.15
Fe	26	8.14	0.41
Functionalized MWCNT			
C	6	83.05	9.88
O	8	14.45	3.57
N	7	1.43	1.45
Fe	26	1.07	0.05

slight differences between them. Figure 4 shows elemental mapping of the samples, revealing that elements are fairly evenly-distributed on the surface and internally (a) before and (b and c) after functionalization. Results of the element content shown in Table I suggest the iron level reduces to a minimum after acid treatment. This suggests that the hot hydrochloric acid efficiently penetrated into both the MWCNT powder and the freestanding MWCNT bulk material successfully dissolving the iron. Also, the increase of oxygen after functionalization due to oxygen plasma treatment is clear, because the atomic percentage of oxygen jumps from <2% of the total to 14.5%.

MWCNTs are generally hydrophobic because they are purely based on aromatic, non-polar, sheets, so that interaction with extremely polar molecules such as water is very weak, unless they have been functionalized with polar moieties. An oxidation

process is one of the easiest ways to functionalize them, making their walls and tips much more hydrophilic. So, the more oxygen functional groups present, the more hydrophilic the sample, at least up to the level measured. The oxygen plasma treatment causes oxygen to attach three-dimensionally on MWCNT powder, presumably helped by the stirring process in the hollow cathode of PECVD reactor. Conversely, for freestanding MWCNT samples, oxygen attaches mainly on the top and bottom surfaces. Although slightly different, both methods efficiently increase the wettability of the freestanding MWCNT and the solubility of the MWCNT powder. The contact angle between the water drop and the sample surface were $\sim 151^\circ$ before and $\sim 0^\circ$ after functionalization, indicating superhydrophobic and superhydrophilic behaviour, respectively. After functionalization, the water droplet instantaneously spreads over the sample surface, indicating

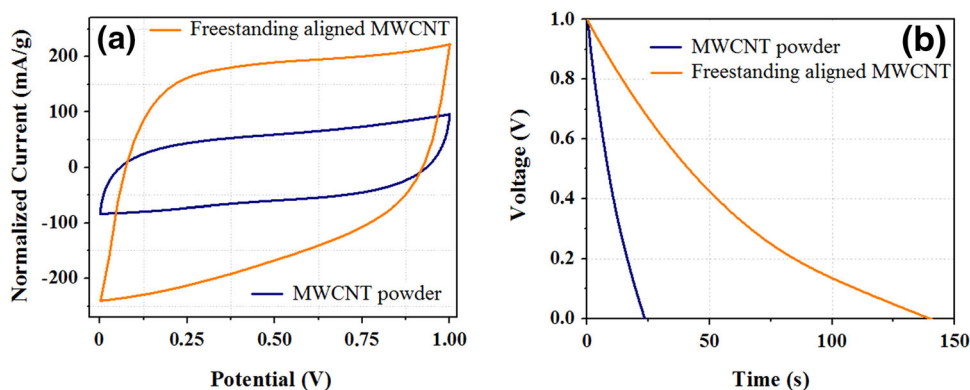


Fig. 5. (a) Cyclic voltammograms scanned at 100 mV s^{-1} and (b) constant-current at 40 mA g^{-1} from MWCNT powder and aligned freestanding materials.

Table II. Specific capacitance, gravimetric specific energy and power from carbon-based supercapacitor devices

Measure	Freestanding aligned MWCNT	MWCNT powder
Specific capacitance (F g^{-1})	1	0.3
Charge efficiency (%)	83.3	64.2
Gravimetric specific energy (W h kg^{-1})	0.28	0.04
Gravimetric specific power (W kg^{-1})	7.2	5.76

MWCNT multi-walled carbon nanotubes.

an extremely hydrophilic surface. This is consistent with a recent report where we showed that the oxygen plasma treatment improves the dispersion of MWCNT powder in water, forming a moderately stable solution.^{26,34}

All properties presented are important for the capacitance of the bulk material in supercapacitor devices, where major differences in the properties of the powder and the freestanding aligned MWCNT were observed.

Electrochemical Behaviour

Figure 5a and b shows the CVs from MWCNT electrodes in the electrochemical supercapacitor cell (Fig. 1) at similar film thicknesses. The CVs have a “quasi-rectangular” shape, which is typical of interfacial double-layer (DL) charging in a non-Faradaic process. The DL charging is due to the formation of a Stern layer at the material electrolyte interface. A Stern layer is defined as a compact layer of immobile ions strongly adsorbed to the electrode surface.¹⁹ There are no free charges within the Stern layer and beyond there is a diffuse layer where ions are mobile under the coupled influence of electrostatic forces and diffusion.¹⁹

Figure 5a contrasts the capacitive behaviour of the MWCNT powder and freestanding aligned electrodes taken from CVs at 100 mV s^{-1} . The specific capacitance (SC) values were $\sim 0.7 \text{ F g}^{-1}$

and $\sim 2 \text{ F g}^{-1}$ for MWCNT powder and freestanding aligned electrodes, respectively. CV measurements were taken with scan rates from 1 mV s^{-1} to 1000 mV s^{-1} . These confirmed that the SCs are constant for low scan rates and correspond to the capacitance under equilibrium conditions. The symmetry in the CV curves is assigned to nearly instantaneous response of ion transport to the variation in electric potential for a large ion diffusion coefficient, which means smaller ionic resistance of the cell.¹⁹ The SC values obtained from discharge measurement (Fig. 5b) were $\sim 0.3 \text{ F g}^{-1}$ and $\sim 1 \text{ F g}^{-1}$ for MWCNT powder and freestanding aligned devices, respectively. This confirms the SC value of each electrode is double the SC value from the respective device, indicating the two symmetrical electrodes are in series.

Table II shows SC, gravimetric specific energy and power from MWCNT supercapacitor devices at similar operation conditions determined from Fig. 5b. The SC calculated from discharging (Fig. 5b) is similar to those obtained from CVs (Fig. 5a). The charge efficiency is much higher for the device fabricated from freestanding material, which means the storage process is more efficient for the energy available, probably due to the interconnected electrode network. Furthermore, our results indicate that the SC, energy and power supplied are higher for supercapacitor devices fabricated with freestanding aligned MWCNT electrodes.

Table III. Supercapacitor data from different manufacturers

Manufacturer	Cell voltage (V)	Gravimetric specific energy (W h kg ⁻¹)
APowerCap ³⁵	2.7	≤4.5
Illinois ³⁶	2.3/2.7	≤6.6
Ioxus ³⁷	2.7	≤6.4
JSR Micro ³⁸	3.8	≤12
Korchip ³⁹	2.5/2.7	≤6.1
Maxwell ⁴⁰	2.2/2.8	≤6.0
Murata ⁴¹	4.2/5.5	≤3.1
Nesscap ⁴²	2.7	≤4.5
	2.3	≤8.7
Samwha ⁴³	2.5/2.7	≤7.0
Skeleton ⁴⁴	2.85	≤10.1
VinaTech ⁴⁵	2.3/3.0	≤6.3

All MWCNT powder electrodes with fairly high mass (25 mg) showed some resistivity, due to the percolation process of charge transport. The energy dissipation takes place at the many carbon and solution solid/solid interfaces, which form ohmic junctions during the percolation processes. It is also feasible that many particles could be inside the porous structure without participating in the charge transport or the double-layer formation. Our results show aligned MWCNT arrays seem to be the better option as electrodes, as they are more resistant to being scratched and delamination. Table III presents data from some of the commercially available supercapacitors. As one can observe the gravimetric specific energy is about an order of magnitude higher than that which we obtained in this work. That was expected considering that the voltage range is exponentially proportional to gravimetric specific energy as presented in the introduction section, and all data in Table III comes from a cell that could reach ~2.7 V. To work in this potential window, organic electrolytes such as TEABF₄/ACN are needed and that is our next target of development.

In general, the high-power discharges obtained from the supercapacitors are directly related to the absence of charge-transfer resistance, which is characteristic of battery Faradaic reactions.³ Supercapacitors occupy a region between batteries and dielectric capacitors on the Ragone plot, describing the relation between gravimetric specific energy and power.³ They have been touted as a solution to the mismatch between the fast growth in power required by devices and the inability of batteries to efficiently discharge at high rates.

CONCLUSION

We have presented an electrochemical double-layer capacitor prepared from MWCNT electrodes for application as supercapacitor devices. Freestanding aligned MWCNT electrodes showed a higher SC and gravimetric specific energy and power than the randomly packed nanoparticle-

based electrodes, probably due to better electron and ion transport during the charge-discharge processes. Our results show that very low-cost MWCNTs are fairly efficient for supercapacitor fabrication, and showed high SC, gravimetric specific energy and power, which could make them complementary to batteries. The next steps are to prepare higher surface-area electrodes and explore pseudocapacitance opportunities such as PANI, Li ion intercalation and ionic liquids for a higher working potential window.

ACKNOWLEDGEMENT

We would like to thank the LME/LNLS-Campinas and University of Bristol for microscope facilities and also NANOBIIO for the AutoLab facility. We gratefully acknowledge the Brazilian agency Fapesp (2014/02163-7, 2015/50093-0, 2014/21587-2, 2015/17829-3, 2015/17764-9) and the Royal Society for Newton Travel fund NI140181 for financial support.

REFERENCES

1. J.-H. Kim, K. Zhu, Y. Yan, C.L. Perkins, and A.J. Frank, *Nano Lett.* 10, 4099 (2010).
2. F.I. Dar, K.R. Moonoswamy and M. Es-Souni, *Nanoscale Res. Lett.* 8, 363 (2013).
3. J. Chmiola, G. Yushin, Y. Gogotsi, C. Portet, P. Simon, and P.L. Taberna, *Science* 313, 1760 (2006).
4. R.S. Borges, A.L.M. Reddy, M-T.F. Rodrigues, H. Gullapalli, K. Balakrishnan, G.G. Silva and P.W. Ajayan. *Sci. Rep.* 3, 2572 (2013).
5. P.H. Chen and R.L. McCreery, *Anal. Chem.* 68, 3965 (1996).
6. J.M. Nugent, K.S.V. Santhanam, A. Rubio, and P.M. Ajayan, *Nano Lett.* 1, 91 (2001).
7. M. Terrones, *Annu. Rev. Mater. Res.* 33, 501 (2003).
8. H. Zanin, A. Margraf-Ferreira, N.S. da Silva, F.R. Marciano, E.J. Corat, and A.O. Lobo, *Mater. Sci. Eng. C Mater. Biol. Appl.* 41, 65 (2014).
9. M.A.V.M. Grinet, H. Zanin, A.E.C. Granata, M. Porcionatto, F.R. Marciano, and A.O. Lobo, *J. Mater. Chem. B* 2, 1196 (2014).
10. T.W. Ebbesen and P.M. Ajayan, *Nature* 358, 222 (1992).
11. K.P. De Jong and J.W. Geus, *Rev. Sci. Eng.* 42, 481–510 (2000).
12. R.L. Vander Wal, T.M. Ticich, and V.E. Curtis, *J. Phys. Chem. B* 104, 11611 (2000).

13. P.M. Ajayan, J.M. Nugent, R.W. Siegel, B. Wei, and P. Kohler-Redlich, *Nature* 404, 243 (2000).
14. D.L. Lichtenberger, K.W. Nebesny, C.D. Ray, D.R. Huffman, and L.D. Lamb, *Chem. Phys. Lett.* 176, 208 (1991).
15. Q.L. Zhang, S.C. O'Brien, J.R. Heath, Y. Liu, R.F. Curl, and H.W. Kroto, *J. Phys. Chem.* 90, 528 (1986).
16. V.L. Kuznetsov, A.L. Chuvilin, Y.V. Butenko, I.Y. Malkov, and V.M. Titov, *Chem. Phys. Lett.* 222, 348 (1994).
17. J.Y. Miao, D.W. Hwang, K.V. Narasimhulu, P.-I. Lin, Y.-T. Chen, S.-H. Lin and L.-P. Hwang, *Carbon* 42, 813 (2004).
18. D. Ugarte, *Nature* 359, 709 (1992).
19. H. Wang and L. Pilon, *Electrochim. Acta* 64, 139 (2012).
20. M.D. Stoller and R.S. Ruoff, *Energy Environ. Sci.* 3, 1294 (2010).
21. D.W. Wang, F. Li, M. Liu, G.Q. Lu, and H.M. Cheng, *Angew. Chem. Int. Ed.* 48, 1525 (2009).
22. L. Demarconnay, E. Raymundo-Pinero, and F. Beguin, *Electrochem. Commun.* 12, 1275 (2010).
23. S. Biswas and L.T. Drzal, *Chem. Mater.* 22, 5667 (2010).
24. D. Ge, L. Yang, L. Fan, C. Zhang, X. Xiao, Y. Gogotsi, and S. Yang, *Nano Energy* 11, 568 (2015).
25. I.A.W.B. Siqueira, C.A.G.S. Oliveira, H. Zanin, M.A.V.M. Grinet, A.E.C. Granato, M.A. Porcionatto, F.R. Marciano, and A.O. Lobo, *J. Mater. Sci. Mater. Med.* 26, 10 (2015).
26. H. Zanin, P.W. May, A.O. Lobo, E. Saito, J.P.B. Machado, G. Martins, V.J. Trava-Airoldi, and E.J. Corat, *J. Electrochem. Soc.* 161, H290 (2014).
27. E.R. Edwards, E.F. Antunes, E.C. Botelho, M.R. Baldan, and E.J. Corat, *Appl. Surf. Sci.* 258, 641 (2011).
28. T.A. Silva, H. Zanin, F.C. Vicentini, E.J. Corat, and O. Fatibello-Filho, *Analyst* 139, 2832 (2014).
29. Y. Li, K. Sheng, W. Yuan, and G. Shi, *Chem. Commun.* 49, 291 (2013).
30. E.F. Antunes, A.O. Lobo, E.J. Corat, V.J. Trava-Airoldi, A.A. Martin, and C. Verissimo, *Carbon* 44, 2202 (2006).
31. M.S. Dresselhaus, A. Jorio, M. Hofmann, G. Dresselhaus, and R. Saito, *Nano Lett.* 10, 751 (2010).
32. A.C. Ferrari, *Solid State Commun.* 143, 47 (2007).
33. H. Zanin, E. Saito, H.J. Ceragioli, V. Baranauskas, and E.J. Corat, *Mater. Res. Bull.* 49, 487 (2014).
34. H. Zanin, L.M. Hollanda, H.J. Ceragioli, M.S. Ferreira, D. Machado, M. Lancellotti, R.R. Catharino, V. Baranauskas, and A.O. Lobo, *Mater. Sci. Eng. C Mater. Biol. Appl.* 39, 359 (2014).
35. APowerCap Technologies, Products. <http://www.apowercap.com/?pg=18&lang=eng&rand=95679520>. Accessed 16 July 2016.
36. Illinois Capacitor, EDLC/SUPERCAPACITORS. <http://www.illinoiscapacitor.com/products/super-capacitors.aspx>. Accessed 16 July 2016.
37. Ioxus, OUR CELLS. <http://www.ioxus.com/english/products/cells/>. Accessed 16 July 2016.
38. JSR Micro, Lithium Ion Capacitor. <http://www.jsrmicro.com/index.php/EnergyAndEnvironment/LithiumIonCapacitor/>. Accessed 16 July 2016.
39. Korchip, StartCap. <http://www.korchip.com/eng/>. Accessed 16 July 2016.
40. Maxwell ultracapacitors: enabling energy's future. Ultracapacitor overview. <http://www.maxwell.com/products/ultracapacitors/>. Accessed 16 July 2016.
41. Murata, Supercapacitors (EDLC). <http://www.murata.com/products/capacitor/edlc>. Accessed 16 July 2016.
42. Nesscap, Overview. <http://www.nesscap.com/product/overview.jsp>. Accessed 16 July 2016.
43. Masters, Green Caps. <http://www.masters.com.pl/files/ds/samwha/samwha-green-cap.pdf>. Accessed 16 July 2016.
44. Skeletontech, Our Technology. <http://www.skeletontech.com/technologies>. Accessed 16 July 2016.
45. Vina Tech, Supercapacitorvina. <http://www.supercapacitorvina.com/?kattempt=1>. Accessed 16 July 2016.